Correspondence to:
S. Gu and Z. Liu,
gusifan@ouc.edu.cn;
liu.7022@osu.edu

Assessing the Ability of Zonal $\delta^{18}O$ Contrast in Benthic Foraminifera to Reconstruct Deglacial Evolution of Atlantic Meridional Overturning Circulation

Sifan Gu[1,2] ![ID], Zhengyu Liu[3], Jean Lynch-Stieglitz[4] ![ID], Alexandra Jahn[5] ![ID], Jiaxu Zhang[6] ![ID], Keith Lindsay[7], and Lixin Wu[1,8]

[1]Physical Oceanography Laboratory, Ocean University of China, Qingdao, China, [2]Open Studio for Ocean-Climate-Isotope Modeling, Pilot National Laboratory for Marine Science and Technology (Qingdao), Qingdao, China, [3]Atmospheric Science Program, Department of Geography, The Ohio State University, Columbus, OH, USA, [4]School of Earth and Atmospheric Sciences, Georgia Institute of Technology, Atlanta, GA, USA, [5]Department for Atmospheric and Oceanic Sciences and Institute of Arctic and Alpine Research, University of Colorado Boulder, Boulder, CO, USA, [6]Computational Physics and Methods (CCS-2) and Center for Nonlinear Studies (CNLS), Los Alamos National Laboratory, Los Alamos, NM, USA, [7]National Center for Atmospheric Research, Climate and Global Dynamics Division, Boulder, CO, USA, [8]Pilot National Laboratory for Marine Science and Technology (Qingdao), Qingdao, China

Abstract $\delta^{18}O$ in foraminifera ($\delta^{18}O_c$) is a useful proxy for density, and the strength of the Atlantic Meridional Overturning Circulation (AMOC) can be reconstructed by the zonal density contrast in the Atlantic. However, whether the deglacial zonal $\delta^{18}O_c$ contrast can represent the AMOC change is still unclear. $\delta^{18}O_c$ contrast across the Florida Straits has been hypothesized as a proxy for the AMOC evolution during the last deglaciation, but the strength of Florida Current could also be influenced by wind forcing. Here we examine the ability of the zonal $\delta^{18}O_c$ contrast to reconstruct AMOC in a deglacial model simulation. The model simulation suggests that the deglacial variation of the Florida Current strength is dominated by AMOC, with the wind effect on the variation of the Florida Current being negligible. Furthermore, the $\delta^{18}O_c$ contrast across the western boundary along the entire Atlantic and the basin-wide $\delta^{18}O_c$ contrast in the North Atlantic in the upper ocean can also be used to reconstruct AMOC. However, using basin-wide $\delta^{18}O_c$ contrast to reconstruct AMOC in the South Atlantic is not possible at all water depths. In the subtropical South Atlantic, the basin-wide $\delta^{18}O_c$ contrast is decoupled from the density contrast between 400 to 600 m through the deglaciation because of the deglacial change of the Antarctic Intermediate Water. Therefore, $\delta^{18}O_c$ is a useful proxy to reconstruct past density and in turn past AMOC, but caution has to be used when using the basin-wide $\delta^{18}O_c$ contrast to reconstruct the basin-wide density contrast in the South Atlantic.

1. Introduction

The Atlantic Meridional Overturning Circulation (AMOC) is one of the most important components of the climate system because of its role in redistributing heat, carbon, and nutrients. Today, AMOC has a two-cell structure: an upper cell where the northward flowing warm surface and intermediate water (upper 1,000 m) loses buoyancy in the North Atlantic and descends to become the southward flowing cold North Atlantic Deep Water (NADW; 1,500–4,500 m) and a lower cell where the Antarctic Bottom Water formed in the Southern Ocean flows northward, mixes with the NADW, and ultimately returns to the Southern Ocean via isopycnal upwelling.

Abrupt climate changes during the last deglaciation are suggested to be associated with changes in AMOC (e.g., Clark et al., 2002; McManus et al., 2004). Several different proxies have been used to reconstruct the paleo-AMOC changes. Nutrient proxies such as $\delta^{13}C$ (Curry & Oppo, 2005), Cd/Ca (e.g., Boyle & Keigwin, 1987; Keigwin & Lehman, 1994), Ba/Ca (Lea & Boyle, 1990), and Zn/Ca (Marchitto et al., 2002) have been used to provide information about the water mass distributions, that is, the structure of the AMOC. But they do not provide an assessment of the strength of the AMOC (LeGrand & Wunsch, 1995). Sediment $^{231}Pa/^{230}Th$ has been proposed as a kinematic tracer for AMOC (Marchal et al., 2000; McManus et al., 2004; Yu et al., 1996), but this approach has been contested because the sediment $^{231}Pa/^{230}Th$ is also influenced by particle flux and composition and its variation differ significantly in different regions in the Atlantic (e.g., Chase et al., 2002).

Basin-wide density contrasts at 26.5°N can be used to monitor AMOC in the modern ocean (Cunningham et al., 2007), and a modeling study suggests that AMOC variability can be reconstructed from basin-wide density contrast (Hirschi & Lynch-Stieglitz, 2006). This is possible because, assuming geostrophic and hydrostatic balance, by integrating the thermal wind balance from the west (Xw) to the east (Xe):

$\int_{X_W}^{X_E} -\frac{f\rho_0}{g}\frac{\partial v}{\partial z}dx = \int_{X_W}^{X_E} \frac{\partial \rho}{\partial z}dx$, the horibalance from thean reflects the zonally averaged vertical shear at this

depth: $-\frac{f\rho_0}{g}L_x\frac{\partial v^-}{\partial z} = \rho_E - \rho_W$, where f is the Coriolis parameter, ρ is seawater density, L_x is the horizontal width, and v is the meridional velocity. The large-scale northward surface flow and southward deep flow of AMOC is reflected in the basin-wide density contrast: The eastern margin is lighter than the western margin in the North Atlantic and vice versa in the South Atlantic (Olbers et al., 1992). Paleodensity can be reconstructed by oxygen isotopic composition in the benthic foraminifera ($\delta^{18}O_c$; Lynch-Stieglitz et al., 1999a, 1999b) because $\delta^{18}O_c$ is determined by the temperature and $\delta^{18}O$ of seawater ($\delta^{18}O_w$), which generally covaries with salinity in the upper ocean. That is, both $\delta^{18}O_c$ and density increase with the increase of salinity and decrease of temperature. Therefore, the basin-wide $\delta^{18}O_c$ contrast in the upper Atlantic has been hypothesized to be a direct proxy for the strength of the AMOC through its northward flowing upper branch (e.g., Lynch-Stieglitz et al., 2007).

This hypothesis of the zonal $\delta^{18}O_c$ contrast as a proxy of AMOC transport, however, is not always consistent with other proxies. The $\delta^{18}O_c$ contrast at 27°S across the Atlantic basin in the upper 2 km has been used to reconstruct the AMOC during the Last Glacial Maximum (LGM; Lynch-Stieglitz et al., 2007). During the LGM, water mass tracers, such as Cd/Ca and $\delta^{13}C$, suggest that AMOC was shallower than present day, with the southward NADW replaced by the Glacial North Atlantic Intermediate Water (Boyle & Keigwin, 1987; Curry & Oppo, 2005; Thomas M. Marchitto & Broecker, 2006). The ratio of $^{231}Pa/^{230}Th$ in deep-sea sediments as well as grain-size analyses along the western boundary have been interpreted as suggesting a vigorous overturning of the Glacial North Atlantic Intermediate Water at the LGM (Bradtmiller et al., 2014; Evans & Hall, 2008; Gherardi et al., 2009; Lippold et al., 2012). This would suggest that there was a much larger vertical shear and therefore larger density contrast across the Atlantic basin during the LGM than at present day. However, $\delta^{18}O_c$ reconstructions suggest a reduced and even reversed $\delta^{18}O_c$ contrast between the eastern and western margin in the upper ocean at 27°S (Lynch-Stieglitz et al., 2006). Hence, if the $\delta^{18}O_c$ contrast represents the density contrast, it is incompatible with the shallower and active AMOC suggested by the other proxies. Therefore, it has remained unclear if the zonal $\delta^{18}O_c$ contrast in the South Atlantic can in fact be used as a proxy for the AMOC evolution. One possibility is at certain times, such as the LGM, the $\delta^{18}O_c$ contrast no longer represents the density contrast because of different water mass properties between the eastern and western margin in the South Atlantic (Gebbie & Huybers, 2006).

The relationship between the horizontal density contrast and the vertical shear is also applicable to flow across ocean gateways (Moreno-Chamarro et al., 2017). For example, the $\delta^{18}O_c$ contrast across the Florida Straits has been used to reconstruct the Florida Current during the last deglaciation. The Florida Straits $\delta^{18}O_c$ contrast shows a substantial reduction during the Younger Dryas (YD; 12.8–11.7 ka), which indicates a reduced horizontal density contrast and therefore the weakening of the Florida Current (Lynch-Stieglitz et al., 2011). The decrease in $\delta^{18}O_c$ contrast over Heinrich Stadial 1 (HS1;17.5–14.7 ka) on the Florida margin suggests that HS1 is also associated with a reduction in the Florida Current (Lynch-Stieglitz et al., 2014). The AMOC transport evolution estimated from the $\delta^{18}O_c$ contrast across Florida Current therefore seems to be consistent with that inferred from other kinematic water tracers, such as sediment $^{231}Pa/^{230}Th$ over the deglaciation (McManus et al., 2004). This is possible because the Florida Current forms part of the upper limb of the AMOC, and therefore, its strength is related to the AMOC strength. However, dynamically, the Florida Current strength can also be influenced by the surface wind stress curl. The present-day Florida Current includes a wind-driven gyre component of ~17 Sv and an AMOC component of ~13 Sv (Schmitz William & McCartney, 1993). It is therefore not obvious that one can ignore the wind effect to conclude that the reduced $\delta^{18}O_c$ contrast across the Florida Straits during the HS1 and the YD simply reflects a reduced AMOC contribution (Lynch-Stieglitz et al., 2014).
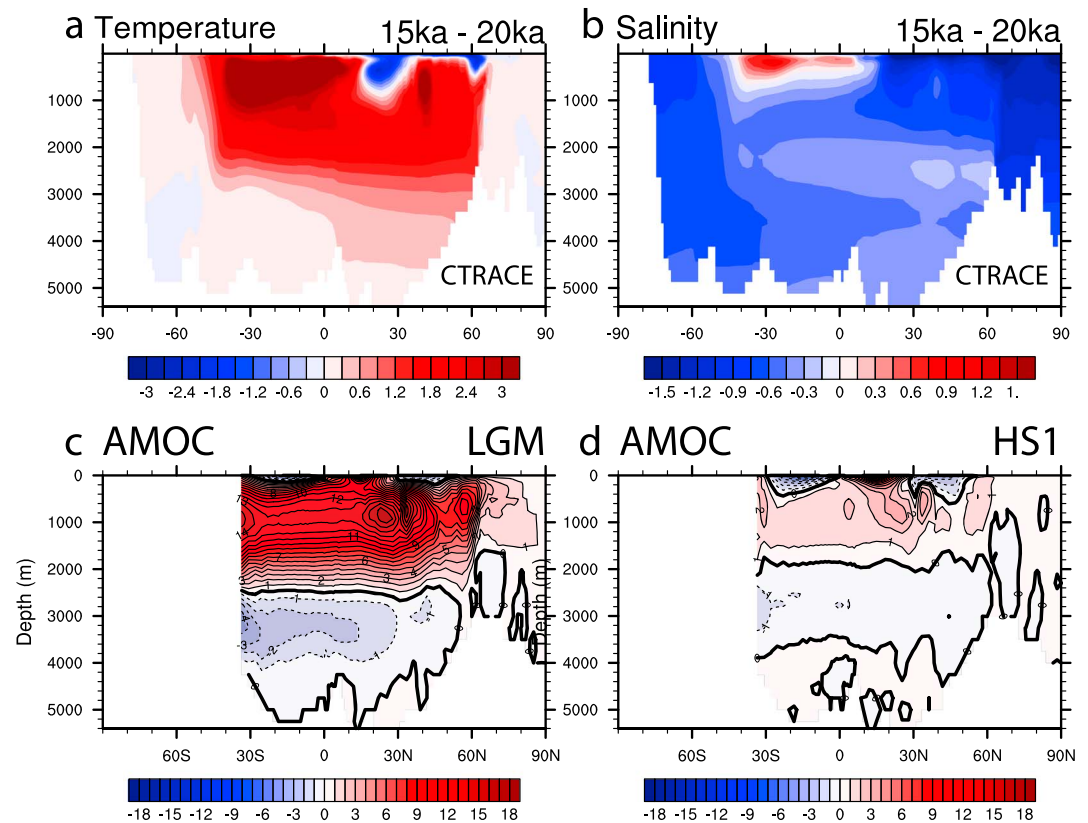
Figure 1. Atlantic zonal mean (a) temperature and (b) salinity difference between 15 and 20 ka in C-iTRACE. AMOC during the (c) LGM (20 ka) and the (d) HS1 (15 ka) in C-iTRACE. AMOC = Atlantic Meridional Overturning Circulation; LGM = Last Glacial Maximum.

Here, we test the hypothesis that the zonal $\delta^{18}O_c$ contrast can be used to reconstruct past AMOC in a comprehensive ocean model. Specifically, we will examine the $\delta^{18}O_c$ and its relationship with AMOC in a transient ocean simulation of the last deglaciation using an isotope-enabled ocean model. We find that in the deglacial model simulation, the $\delta^{18}O_c$ contrast across the Florida Straits indeed represents the change of AMOC, with little impact from the wind-driven circulation. Furthermore, the zonal $\delta^{18}O_c$ contrast that are used to reconstruct the western boundary current (WBC) can be used to infer changes in the AMOC strength. However, in our model simulation, the relationship between the $\delta^{18}O_c$ contrast across the whole Atlantic basin and the AMOC depends on the latitude and depth. In particular, this relationship fails in the South Atlantic because of a large change in Antarctic Intermediate Water (AAIW) properties.

2. Model and Experiment

We employ the isotope-enabled Parallel Ocean Program version 2 (iPOP2) to simulate the deglacial ocean evolution in this study. iPOP2 is the ocean component of the Community Earth System Model, and the details of the physical ocean model are described in Danabasoglu et al. (2012). The ocean model configuration in this study has a nominal 3° horizontal resolution and 60 vertical layers, with 10-m resolution in the upper 200 m, expanding to 250-m resolution below 3,000 m. To allow for a direct model-data comparison, several widely used geotracers have been implemented in iPOP2, such as $\delta^{18}O$ (Zhang et al., 2017), $^{231}Pa/$ ^{230}Th (Gu & Liu, 2017), ε_{Nd} (Gu et al., 2017), $\delta^{13}C$, and radiocarbon (Jahn et al., 2015). These geotracers make iPOP2 a useful tool for paleoclimate research.

To study the deglacial $\delta^{18}O_c$ contrast and AMOC in the Atlantic, we performed a transient ocean simulation with iPOP2 (C-iTRACE) from 20 to 11 ka. C-iTRACE is forced by the monthly fluxes of momentum, heat, freshwater, and sea ice fractions from a fully coupled transient simulation of the last deglaciation using the Community Climate System Model version 3 (CCSM3; TRACE21), which has been shown to
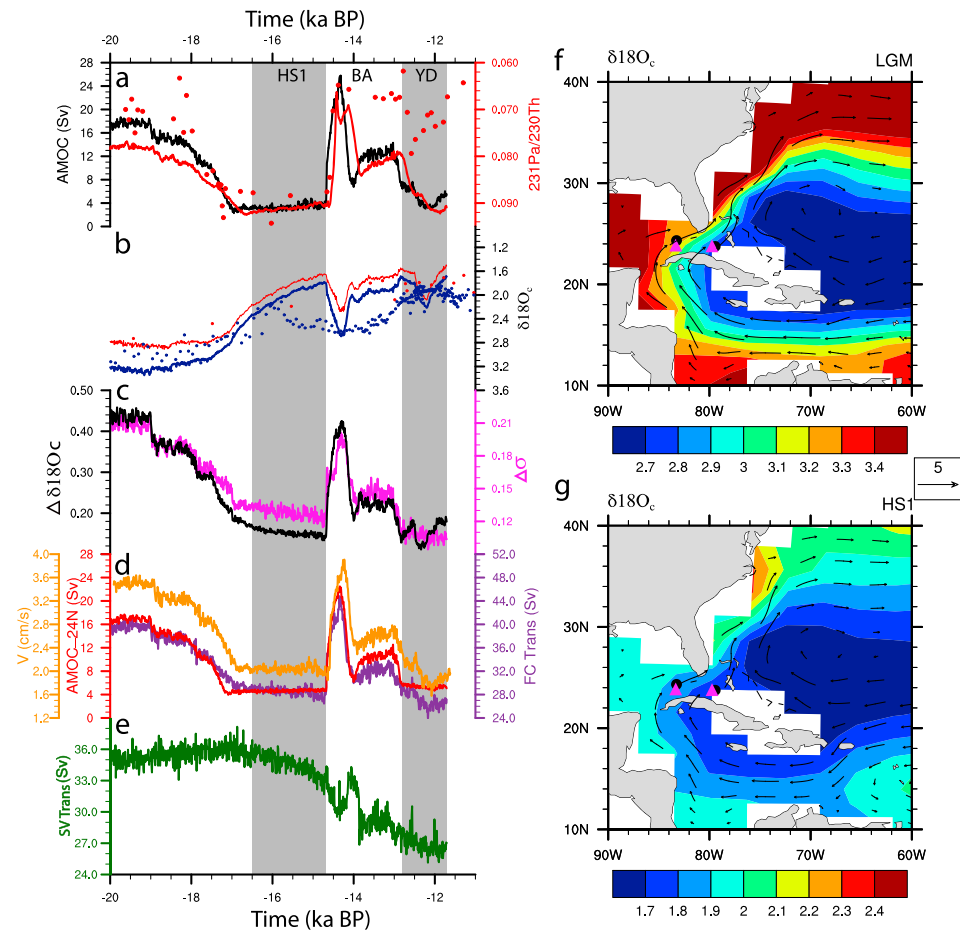
Figure 2. Time evolutions in the Florida Straits and the $d^{18}O_c$ distribution in C-iTRACE. (a) AMOC strength (black) and observational (red dot; McManus et al., 2004) and model (red curve) $^{231}Pa/^{230}Th$ from site OCE326-GGC5 (33°42′N, 57°35′W, 4.55 km). The strength of AMOC is defined as the maximum of the Atlantic meridional overturning stream function below 500 m between 30°N and 60°N (in Sverdrup, Sv). (b) $\delta^{18}O_c$ evolution from two cores located on either side of the Florida Current (blue for the west site; red for the east site). Dots are observations (Lynch-Stieglitz et al., 2014), and curves are model results. The location of the two observational sites in Lynch-Stieglitz et al. (2014) is shown as black circles, and the location of the model grids for these two observational sites are shown as magenta triangles in (f). (c) $\delta^{18}O_c$ contrast (black) and density contrast (magenta) between the two Florida Straits sites in C-iTRACE. (d)The average meridional velocity at 530 m in the Florida Straits (orange), the Florida Current transport (purple), and the maximum of the Atlantic meridional overturning stream function at 24.5°N (red). (e) The Sverdrup transport in the Florida Straits in C-iTRACE. (f) $\delta^{18}O_c$ distribution at 530 m during LGM in C-iTRACE, with velocity overlaid as vectors. (g) The same as (e) for the HS1. AMOC = Atlantic Meridional Overturning Circulation; LGM = Last Glacial Maximum.

reproduce many important features of the deglacial climate changes (P. U. Clark et al., 2012; Z Liu et al., 2009; Zhengyu Liu, Lu, et al., 2014; Marcott et al., 2011; Otto-Bliesner et al., 2014). Following Zhang et al. (2017), a relative strong temperature and salinity restoring to the monthly mean TRACE21 output is applied. The restoring flux is $Q_\varphi = \frac{H}{\tau}(\varphi_o - \varphi_M)$, where H is the effective thickness, τ is the restoring time scale, φ_o is the surface temperature/salinity in TRACE21, and φ_M is the temperature/salinity in C-iTRACE. In Zhang et al., 2017, H is set to be the thickness of the surface layer (10 m) and τ is set to be 10 days for temperature and 30 days for salinity. In this study, we use the local mixed layer depth as H and τ is set to be 30 days for temperature and 60 days for salinity. This mixed layer-dependent restoring produces more realistic subsurface temperatures and salinities in deep convection regions compared with the restoring parameters used in Zhang et al. (2017).

The temperature and salinity fields are initialized from the LGM condition in an ocean simulation, which also uses iPOP2 (Zhang et al., 2017) and are spun up for 4,788 years under LGM condition. We then spun up the $\delta^{18}O$ tracer field for the LGM conditions for 2,000 years, which was initiated from the modern
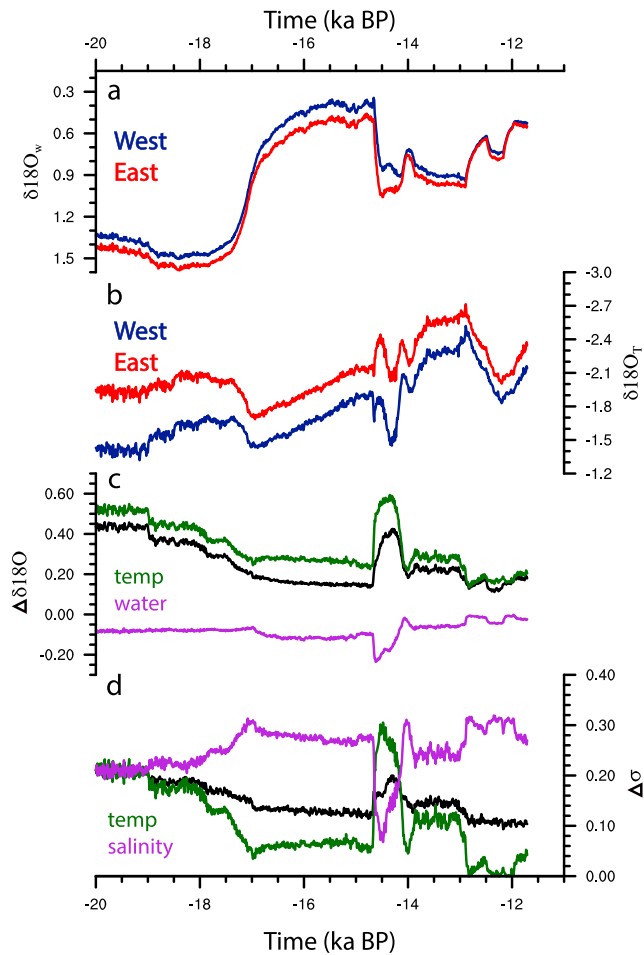
Figure 3. Time evolutions in the Florida Straits. (a) $\delta^{18}O_w$ evolution from the two cores in the Florida Straits (blue for the west site; red for the east site). (b) $\delta^{18}O_T$ evolution from the two cores (navy for the western site; red for the eastern site). (c) The contrast (west-east) of $\delta^{18}O$ between the two cores: black for the $\delta^{18}O_c$, green for $\delta^{18}O_T$, and purple for $\delta^{18}O_w$. (f) The density contrast (west-east) between the two cores (black), the density contrast caused by the salinity contrast (purple), and the density contrast caused by the temperature contrast (green).

$\delta^{18}O$ in Zhang et al. (2017). The transient simulation starts at 20 ka and ends at 11 ka. The surface forcing scheme for $\delta^{18}O$ is exactly the same as in Zhang et al. (2017), which uses the isotopic composition in precipitation and evaporation from snapshot experiments of the last deglaciation with the isotope-enabled atmospheric model (isoCAM3; Zhengyu Liu, Wen, et al., 2014), and sets the $\delta^{18}O$ in the meltwater flux to −31‰ in the Northern Hemisphere starting at 19 ka and −38‰ in the Southern Hemisphere starting at 14.35 ka. The decadal means of the simulation results are used for analysis in this study.

C-iTRACE is able to reproduce the physical ocean evolution of TRACE21. From the LGM to the late HS1 at 15 ka, the temperature and salinity changes in most of the Atlantic in C-iTRACE (Figure 1) resemble closely those in the TRACE21 results (Figure S1 in the supporting information). However, in the Nordic Sea, the temperature and salinity changes in C-iTRACE are quite different from TRACE21, which is probably caused by the surface restoring applied. The surface restoring will correct the surface but will bias the subsurface. The restoring flux depends on the mixed layer depth, and in the Nordic Sea, the mixed layer depth is quite large, which will lead to large restoring flux and increased bias in the subsurface. The AMOC evolution in terms of upper cell and lower cell intensity shows similar evolutions between C-iTRACE and TRACE21 (Figure S1). The upper cell of AMOC reduces during the HS1 due to the freshwater forcing in the North Atlantic, recovers rapidly during the Bølling-Allerød (BA), and reduces again during the YD in C-iTRACE (Figure 2a). Since the $^{231}Pa/^{230}Th$ is also implemented in C-iTRACE (Gu & Liu, 2017), the modeled $^{231}Pa/^{230}Th$ can be directly compared with the sediment $^{231}Pa/^{230}Th$ from Bermuda Rise (McManus et al., 2004; Figure 2a). The change of $^{231}Pa/^{230}Th$ (p-fixed version in Gu & Liu, 2017) in C-iTRACE is generally in good agreement with the observation before the BA. From the BA to the YD, the absolute value of modeled $^{231}Pa/^{230}Th$ is higher than in the observation, but the relative change is still the same. Since the modeled $^{231}Pa/^{230}Th$ evolution closely tracks the AMOC evolution, especially from the LGM to the HS1, it suggests that AMOC in C-iTRACE is a possible match to the real world AMOC evolution during the last deglaciation.

3. Results

3.1. $\delta^{18}O_c$ Contrast in the Florida Straits

C-iTRACE simulates a reduced $\delta^{18}O_c$ contrast across the Florida Straits during the HS1 and the YD, consistent with the observations (Lynch-Stieglitz et al., 2014). The $\delta^{18}O_c$ in the model is calculated from $\delta^{18}O_w$ and temperature by

$$\delta^{18}O_c = \delta^{18}O_w - 0.27 + 0.0011t^2 - 0.245t + 3.58,$$

where t is temperature in degrees Celsius (T. M. Marchitto et al., 2014). In this way, $\delta^{18}O_c$ in the model can be decomposed into the water component ($\delta^{18}O_w$) and the temperature component ($\delta^{18}O_T = 0.0011t^2 - 0.245t$). The $\delta^{18}O_c$ contrast on the two sides of the Florida Current in Lynch-Stieglitz et al. (2014) shows a large reduction during the HS1 and YD (Figure 2b), which is captured by the modeled $\delta^{18}O_c$ (Figure 2c). The two observational cores in Lynch-Stieglitz et al. (2014) are located at two model grids next to each other (Figures 2f and 2g) with the west grid depth of 1,500 m and the east grid depth of 1,100 m.

The deglacial evolution of the $\delta^{18}O_c$ contrast in the Florida Straits follows the changes of the zonal density contrast across the Florida Straits (Figure 2c) because the evolution of both the $\delta^{18}O_c$ contrast and the density contrast are dominated by that of the temperature contrast. The evolution of the contrast of $\delta^{18}O_c$

Table 1
Transports at 20 ka and 15 ka and the Difference Between 20 and 15 ka

Transport	20 ka	15 ka	20–15 ka
Trans(FC)	38.8	28.7	10.1
Trans(Sv)	35.5	34.9	0.6
AMOC(24.5°N)_max	16.1	4.7	11.4

Note. Trans(FC) is the Florida current transport defined in Figure S2. Trans(Sv) is the Sverdrup transport in the Florida Straits. AMOC(24.5°N)_max is maximum of the Atlantic meridional overturning stream function at 24.5°N.

between the two sites is dominated by the change of temperature contrast, which overwhelms the change of $\delta^{18}O_w$ contrast (Figure 3c). This occurs because the deglacial evolution of $\delta^{18}O_w$ is relatively uniform near the WBC region, perhaps due to the mixing by the circulation. Density evolution can also be decomposed into the temperature and salinity components. The density change caused by the temperature is calculated using the deglacial temperature evolution with the salinity fixed at the LGM value and vice versa for the salinity component. Similar to the $\delta^{18}O_c$ contrast, the change of zonal density contrast across the Florida Straits is also dominated by the temperature contrast change, which overwhelms the opposite compensation change associated with the salinity component (Figure 3d). Since both the deglacial $\delta^{18}O_c$ contrast and the density contrast evolutions are dominated by the temperature contrast, the $\delta^{18}O_c$ contrast is a good representation of the density contrast during the last deglaciation in the Florida Straits.

Reduced zonal density contrast during the HS1 and the YD suggests reduced strength of the Florida Current following the thermal wind relationship, which is also confirmed by C-iTRACE (Figure 2d). The average meridional velocity between the two observational sites at 530 m, which is the model level closest to that of the two sites, shows similar evolutions as the density contrast (Figure 2d, orange). In this coarse resolution model, the WBC is not resolved well. To calculate the Florida Current transport, we use the total norward western boundary transport as an approximation (Figure S2). The total northward Florida Current transport is tightly coupled with the evolution of the density contrast (Figure 2d, purple). This is not obvious, physically. As a WBC in the upper ocean which consists partly of the northward upper limb of AMOC (Figure S2), the Florida Current is also influenced by the wind forcing. These two effects are difficult to separate in paleoreconstructions but can be evaluated in our model simulation. We use the maximum of the meridional overturning stream function at 24.5°N as the transport by AMOC at the latitude of the Florida Straits (Figure 2d, red). From the LGM to the late HS1, the total northward Florida Current transport decreases by 10.1 Sv and the transport by AMOC at the latitude of the Florida Straits decreases by 11.4 Sv. The deglacial change of the Florida Current transport can be mostly explained by the AMOC change (Figure 2d), suggesting that the change of wind component is quite small. Another way to evaluate the wind effect is by
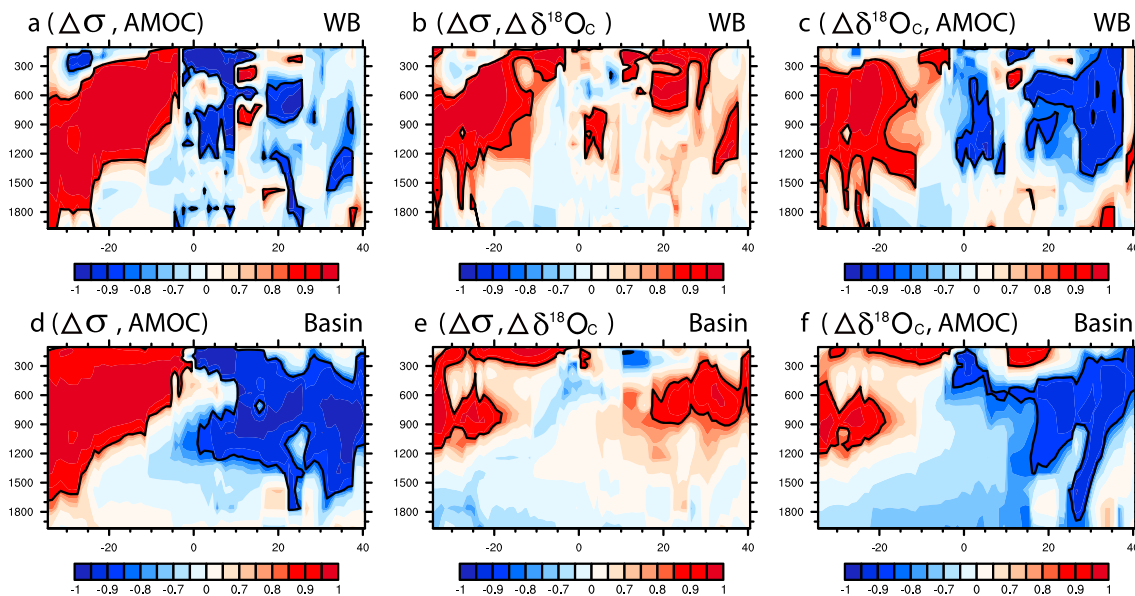

Figure 4. Correlation between the density contrast at different depth, $\delta^{18}O_c$ contrast at different depth and AMOC strength (Figure 2a black AMOC curve) in C-iTRACE. (a) The correlation between AMOC and the density contrast across the WBC region. (b) The correlation between the density contrast and the $\delta^{18}O_c$ contrast across the WBC region. (c) The correlation between $\delta^{18}Oc$ contrast across the WBC region and AMOC. (d)–(f) is the same as (a)–(c) but for the contrast across the Atlantic basin. AMOC = Atlantic Meridional Overturning Circulation.
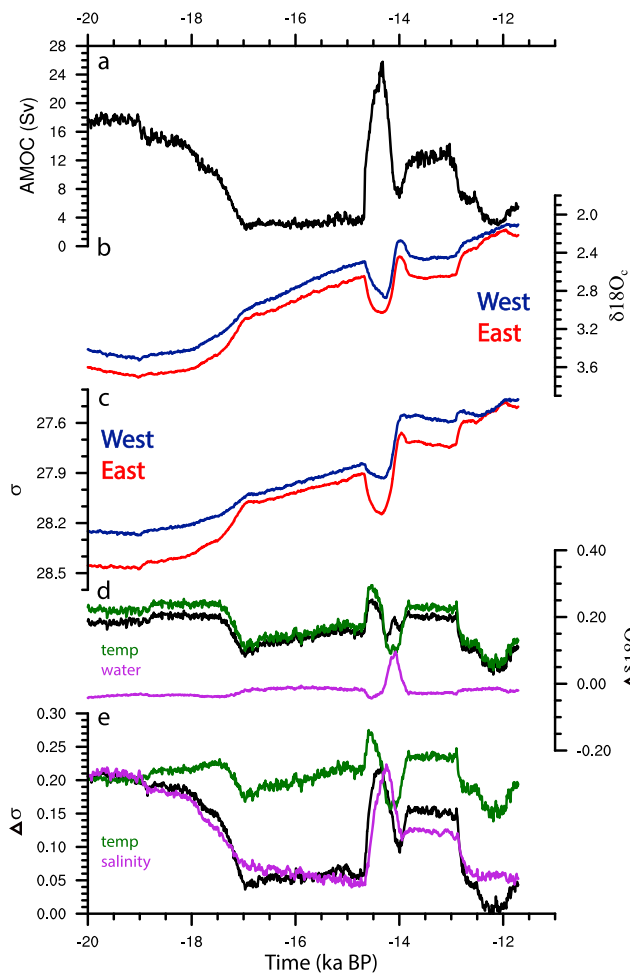
Figure 5. Time evolutions at 530 m at 27°S in C-iTRACE. (a) AMOC strength. (b) $\delta^{18}O_c$ evolution from the western (navy) and eastern (red) margin. (c) Potential density evolution from the western (navy) and eastern (red) margin. (d) The basin-wide contrast (east-west) of $\delta^{18}O$: black for the $\delta^{18}O_c$, green for $\delta^{18}O_T$, and purple for $\delta^{18}O_w$. (e) The potential density contrast (west-east; black), the density contrast caused by the salinity contrast (purple), and the density contrast caused by the temperature contrast (green). AMOC = Atlantic Meridional Overturning Circulation.

calculating the Sverdrup transport, which is to integrate the Sverdrup relation from the eastern boundary to the western boundary. The Sverdrup relation is $\beta V = \frac{\text{curl } \tau}{\rho_0}$, where β is the meridional gradient of the Coriolis parameter, V is the total meridional transport, τ is surface wind stress, and ρ_0 is the average density of seawater (Sverdrup, 1947). In the WBC region, with the continental slope, the effect of the wind-driven circulation is different from ocean interior due to the joint effect of baroclicity and bottom relief (Sarkisyan & Ivanov, 1971). Nevertheless, the Sverdrup transport can be a rough indicator of the wind effect. From the LGM to the last HS1, the Sverdrup transport in the Florida Straits only decreases by 0.6 Sv (Table 1 and Figure 2e), which also implies that the Florida Current transport is mainly dominated by the AMOC and the wind effect is negligible from the LGM to the HS1. Consequently, the surface wind is not the controlling factor of the Florida Current and the Florida Currents strength is a good indicator for AMOC strength from the LGM to the HS1. This is consistent with the strong resemblance of the deglacial evolution of the Florida Current and the AMOC evolution at 24°N (Figure 2d, purple and red). However, during YD from 12.8 to 11.7 ka, AMOC shows no change but the Florida Current transport shows a decrease followed by an increase, which is caused by the surface wind since the Sverdrup transport shows similar changes during this time period. Nevertheless, the major changes of the Florida Current transport during the last deglaciation in C-iTRACE is consistent with the AMOC at 24°N, suggesting that the Florida Current transport is mainly controlled by AMOC. The $\delta^{18}O_c$ contrast covaries with the density contrast in the Florida Straits and represents the strength of Florida Current, which is controlled by AMOC evolution during the last deglaciation. Hence, results from C-iTRACE simulation suggest that the $\delta^{18}O_c$ contrast in the Florida Straits can be used to reconstruct past AMOC during the last deglaciation. Since this evolution is also consistent with other kinematic water tracers, such as sediment $^{231}Pa/^{230}Th$ (McManus et al., 2004), we suggest that this evolution is a robust representation of AMOC during the deglaciation.

3.2. $\delta^{18}O_c$ Contrast Across the Atlantic Basin and the WBC Region

To examine how well the $\delta^{18}O_c$ contrast across the Atlantic basin and the WBC region can be used to reconstruct deglacial AMOC, we analyze the deglacial changes of $\delta^{18}O_c$ contrast and density contrast across both the WBC region and the Atlantic basin in the extratropical Atlantic in the upper ocean at all depths and latitudes. The basin-scale contrast is calculated using the difference between the eastern margin grid and the western margin grid. The contrast in the WBC region is calculated using the difference between the western margin grid and the grid that is 6°E from the western margin. The exceptions are from 22°N to 25°N, where the western margin grid used to calculate the contrast is 6°E from the actual western margin grid and from 26°N to 28°N, where the western margin grid used to calculate the contrast is 14°E from the actual western margin grid. An example of the locations of the model grids used to calculate the contrast at 530 m is illustrated in Figure S3.

In the extratropical region, the density contrast across the WBC region and across the Atlantic basin in the upper ocean is correlated with AMOC during the last deglaciation in both Northern and Southern hemisphere in C-iTRACE. In the WBC region, flow at depths below the major wind-driven boundary current is dominated by the upper northward flowing limb of the AMOC. The density contrast across the WBC can be used to reconstruct the baroclinic velocity by the thermal wind balance. The upper ocean consists of the upper AMOC limb of northward flow above 900 m (Figure S4). The northward meridional velocity at

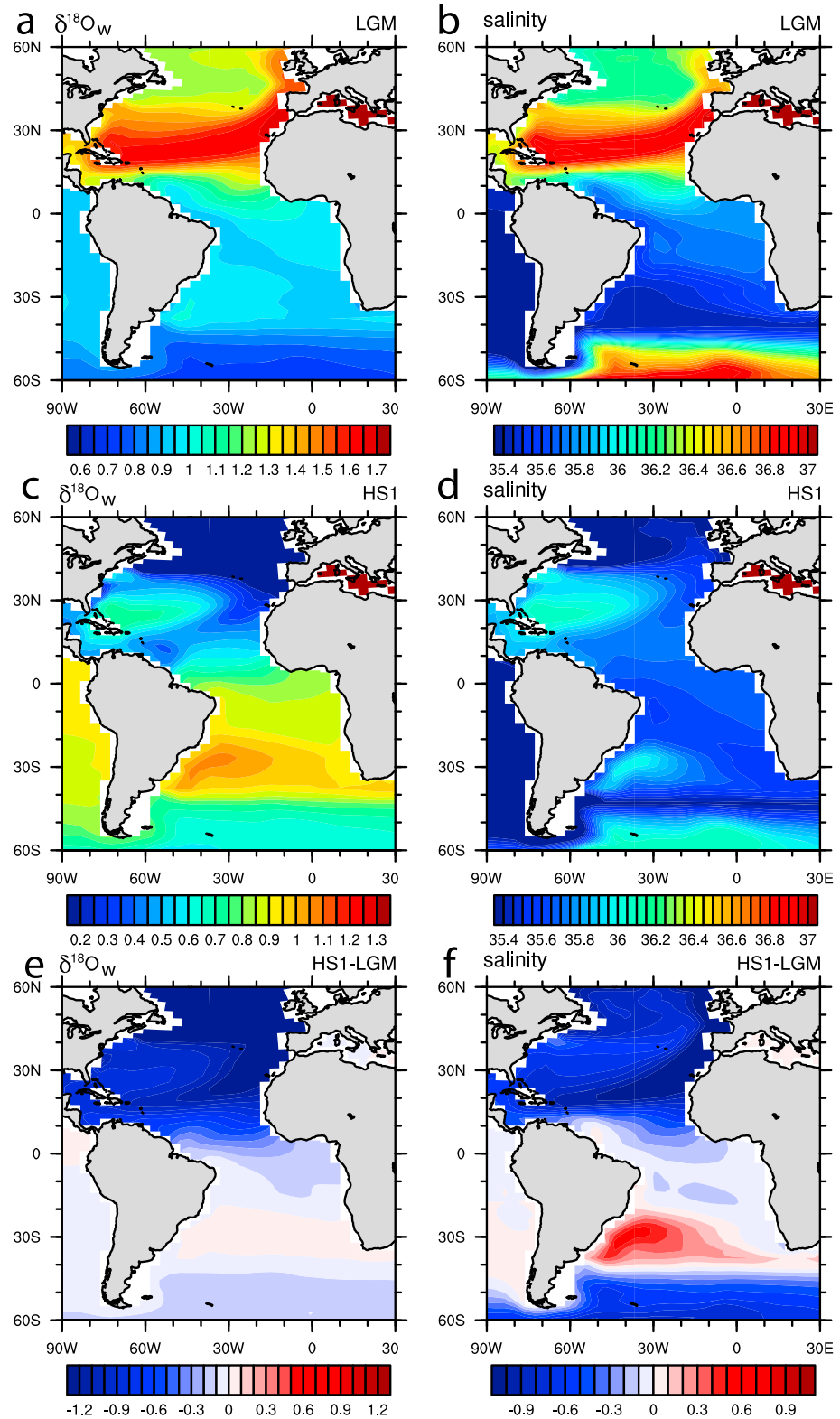**Figure 6.** Distribution of δ^{18}Ow and salinity 530 m in C-iTRACE. (a) δ^{18}Ow during the LGM (20 ka). (b) Salinity during the LGM. (c, d) The same as (a) and (b) for the late HS1 (15 ka). (e, f) The same as (a) and (b) for the difference between the HS1 and the LGM. LGM = Last Glacial Maximum.
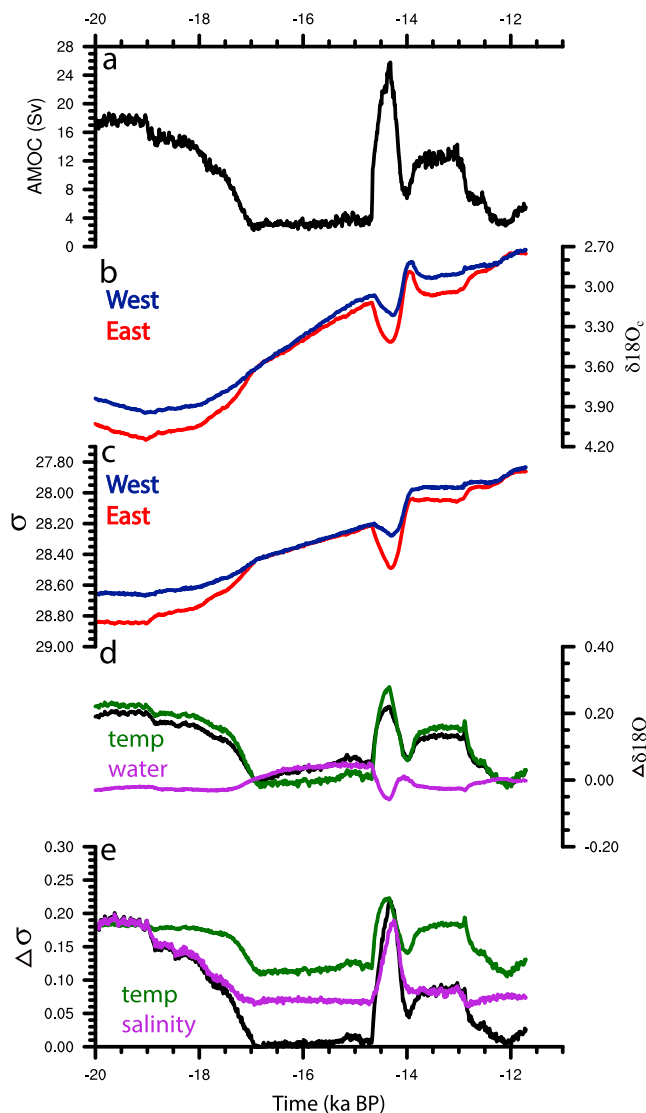
Figure 7. Time evolutions at 878 m at 27°S in C-iTRACE. (a) AMOC strength. (b) $\delta^{18}O_c$ evolution from the western (navy) and eastern (red) margin. (c) Potential density evolution from the western (navy) and eastern (red) margin. (d) The basin-wide contrast (east-west) of $\delta^{18}O$: black for the $\delta^{18}O_c$, green for $\delta^{18}O_T$, and purple for $\delta^{18}O_w$. (e) The potential density contrast (west-east; black), the density contrast caused by the salinity contrast (purple), and the density contrast caused by the temperature contrast (green). AMOC = Atlantic Meridional Overturning Circulation.

20°S shows a positive vertical shear below 300 m in the upper ocean, which is consistent with the high correlation (we define the correlation larger than 0.85 as high correlation) between the density contrast across the WBC region and AMOC strength between 300 to 1,200 m in the southern extratropical region in the Atlantic (Figure 4a). In the Northern Hemisphere, the density contrast across the WBC region shows a more variable correlation with AMOC from 10°N to 20°N than in the South Atlantic (Figure 4a). This is likely contributed by the complicated topographic features and the dominant zonal, rather than meridional, velocity in that region (Figure 2e). However, from 15°N to 25°N, the density contrast across the WBC region is highly correlated with the AMOC from 400 to 900 m in the Florida Current region (Figure 4a), which has been discussed in section 3.2. For the basin-wide density contrast, it is highly correlated with AMOC in both North Atlantic and South Atlantic (Figure 4d) in the upper 1,200 m, following the thermal wind balance (Hirschi & Marotzke, 2007). Therefore, the C-iTRACE simulation suggests that the density contrast across the Atlantic basin and the WBC region in the subtropical Atlantic can be used to reconstruct AMOC in the upper ocean (400 to 900 m).

Now, we turn to the $\delta^{18}O_c$ contrast. First, in the WBC region of both the North and South Atlantic, the $\delta^{18}O_c$ contrast in the upper ocean (400 to 900 m) is highly correlated with the density contrast across the WBC region (Figure 4b) and in turn the WBC. Furthermore, since the WBC in the upper ocean covaries with AMOC (Figure S4), due to the dominance of the upper northward limb of the AMOC, the $\delta^{18}O_c$ contrast across the WBC region also covaries with the AMOC in both the North and South Atlantic (Figure 4c). This suggests that the upper ocean $\delta^{18}O_c$ contrast in the WBC region can be used to reconstruct past changes of not only the WBC in the upper ocean, but also the AMOC in both North and South Atlantic.

Unlike the $\delta^{18}O_c$ contrast across the western boundary, however, using the $\delta^{18}O_c$ contrast across the Atlantic basin to reconstruct the basin-wide density contrast in C-iTRACE is valid for limited depth ranges, from 400 to 900 m in the North Atlantic and from 600 to 900 m in the South Atlantic (Figure 4e). In the North Atlantic, the high correlation between the basin-wide $\delta^{18}O_c$ contrast and the density contrast in the upper ocean suggests that the $\delta^{18}O_c$ contrast across the subtropical Atlantic can be used to reconstruct the basin-wide density contrast and therefore the AMOC during the last deglaciation (Figures 4e and 4f). In comparison, in the South Atlantic, the correlation between the $\delta^{18}O_c$ contrast and the density contrast (or AMOC) is small from 400m to 600m but is high from 600 to 900 m (Figures 4e and 4f), suggesting that the $\delta^{18}O_c$ contrast

no longer evolves with the density contrast (or AMOC) in the South Atlantic from 400 to 600 m but can be used to reconstruct the AMOC at the deeper ranges from 600 to 900 m.

To explore the reason that leads to the decoupling of the basin-wide $\delta^{18}O_c$ gradient from the density gradient from 400 to 600 m in the South Atlantic, we examine the time evolution of the 27°S basin-wide contrast of $\delta^{18}O_c$ at 530 m. The $\delta^{18}O_c$ at both the eastern and western margin evolves with the density (Figures 5b and 5c). However, the $\delta^{18}O_c$ contrast does not evolve with the density contrast, especially from the LGM to the HS1. The $\delta^{18}O_c$ contrast during the HS1 is comparable with that during the LGM, but the density contrast is much smaller during HS1 than the LGM (Figures 5d and 5e). At 19 ka, when the freshwater flux is applied to the North Atlantic, both the AMOC and the basin-wide density contrast start to decrease. However, the $\delta^{18}O_c$ contrast does not decrease; instead, it slightly increases at that time. Although the $\delta^{18}O_c$ contrast
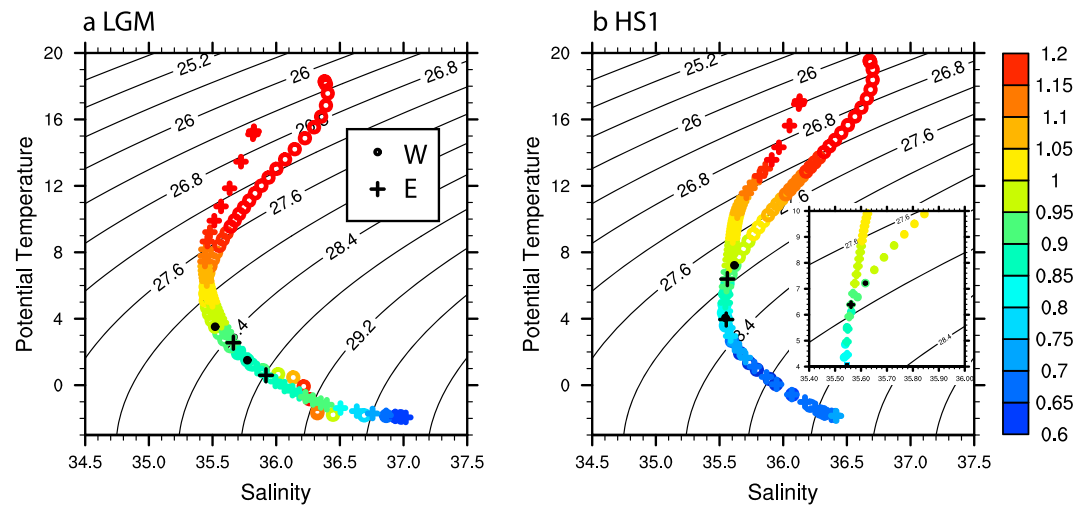
Figure 8. T-S diagram in the western and eastern margin at 27°S in C-iTRACE during the LGM (a) and the HS1 (b). The values of $\delta^{18}O_w$ are indicated by the color. The profile with dots is the western margin profile, and the profile with crosses is the eastern margin profile. The black dots and crosses indicate the value at 530 and 878 m. The enlarged T-S diagram around 530 m is overlaid in (b). LGM = Last Glacial Maximum.

shows a decrease starting at 17.5 ka, it returns to the LGM values in late HS1. Decomposing the density and $\delta^{18}O_c$ contrasts into salinity/$d^{18}O_w$ and temperature components (Figures 5d and 5e) as we did earlier for the Florida Straits, we find the reason of the decoupling of the $\delta^{18}O_c$ contrast from the density contrast at 27°S: The $\delta^{18}O_c$ contrasts are dominated by temperature contrasts, but the density contrasts are dominated by salinity contrasts instead (Figures 5d and 5e). This is also shown in the $\delta^{18}O_w$ and salinity difference maps at the LGM and HS1 at this depth (Figure 6). $\delta^{18}O_w$ shows similar magnitudes of increase across 27°S from the LGM to HS1 (Figure 6e). However, salinity at this depth shows quite a different pattern, with a much larger increase in the western margin than the eastern margin (Figure 6f). During the LGM, the water at 530-m depth is influenced by the AAIW, and the salinity map indicates that the low salinity AAIW circulates in the subtropical gyre in the South Atlantic and penetrates further northward across the equator along the western boundary (Figure 6b). The east-west salinity contrast is therefore positive. However, during HS1, the core of AAIW is shifted to greater depths (Gu et al., 2017) and the salinity distribution at 530 m only shows a narrow band of fresh AAIW at 40°S. Without the influence of the AAIW, the western margin at 27°S experiences salinification, leading to a negative east-west salinity contrast that results in a large reduction of the basin-wide density contrast. It is therefore the large depth change of AAIW in the South Atlantic that causes the decoupling of $\delta^{18}O_w$ and salinity contrasts, so that the $\delta^{18}O_w$ contrast does not predict the AMOC evolution from 400 to 600 m in the South Atlantic. However, the basin-wide $\delta^{18}O_c$ contrast at the same latitude is highly correlated with the density contrast (AMOC) from 600 to 900 m. The similar decomposition of the $\delta^{18}O_c$ contrast and the density contrast at 878 m shows that the $\delta^{18}O_c$ contrast is still controlled by the temperature contrast (Figure 7). The density contrast changes caused by the temperature and by the salinity are in the same direction during the last deglaciation. Therefore, 27°S $\delta^{18}O_c$ contrast at 878 m covaries with the density contrast and in turn with the AMOC change.

Our results suggest that different water masses influencing the western and eastern margin may interrupt the relationship between the density contrast and the $\delta^{18}O_c$ contrast and water mass properties need to be better constrained before using the $\delta^{18}O_c$ contrast to reconstruct the density contrast across the Atlantic basin (Gebbie & Huybers, 2006). During the LGM, both the eastern and western margins at 530 m in the South Atlantic are influenced by the AAIW (Figure 8a). However, during the HS1, both of the eastern and western margin at 530 m are above the AAIW and are influenced by the subtropical water, which shows quite different water mass properties between the eastern and western margin (Figure 8b). In contrast, the depth of 878 m is slightly below the AAIW depth during the LGM but is influenced by AAIW during the HS1 for both the western and eastern margin. In addition, the western and eastern margins show

similar water mass properties from the AAIW depth to the Antarctic Bottom Water depth. Therefore, the basin-wide $\delta^{18}O_c$ contrast is correlated with the density contrast. Because of the long distance between the eastern and western margin, it is much easier to have different water mass properties intruding across the basin than across the WBC region. Furthermore, the strong salinity signature of the AAIW and its large response to deglacial forcing (Gu et al., 2017) makes the upper South Atlantic more vulnerable to water property changes. Therefore, the success of using the $\delta^{18}O_c$ contrast across the Atlantic basin in C-iTRACE to reconstruct the density contrast depends on the depth in the South Atlantic, because of different water mass changes in the eastern and western margin during the last deglaciation.

It should be noted, however, that C-iTRACE cannot reproduce the higher $\delta^{18}O_c$ in the western margin than the eastern margin in the upper ocean as in the reconstructions at the LGM (Lynch-Stieglitz et al., 2007; Figure S5). The distribution of the $\delta^{18}O_c$ in the model during the LGM is consistent with the density distribution, as well as a shallower than present-day but still active AMOC in the model and suggested by other proxy reconstructions (Boyle & Keigwin, 1987; Curry & Oppo, 2005; Thomas M. Marchitto & Broecker, 2006). Hence, the model cannot be used to help resolve the discrepancy between the $\delta^{18}O_c$ and other proxies.

4. Conclusion and Discussion

Results from C-iTRACE simulation confirm that the $\delta^{18}O_c$ in the upper Atlantic (400–900 m) is a useful proxy for reconstructing past density, the northward upper limb of the AMOC, and in turn the AMOC strength. This $\delta^{18}O_c$ proxy for density, however, is not valid everywhere at all times. We show that in C-iTRACE, the $\delta^{18}O_c$ contrast in the Florida Straits reflects the density contrast, and therefore the strength, of the Florida Current. The deglacial variation in the Florida Current is mainly dominated by the AMOC change instead of by surface wind stress. Therefore, the $\delta^{18}O_c$ contrast in the Florida Straits can be used to reconstruct the northward upper limb of the AMOC and, in turn, the AMOC strength, during the last deglaciation. Furthermore, in the upper ocean, our model simulation suggests that the $\delta^{18}O_c$ contrast across the WBC region in general can represent the density contrast evolution during the last deglaciation. However, the relationship between the $\delta^{18}O_c$ contrast and the density contrast across the Atlantic basin depends on the depth. The basin-wide $\delta^{18}O_c$ contrast is highly correlated with the density contrast/AMOC in the North Atlantic from 400 to 900 m. In the South Atlantic, the deglacial basin-wide $\delta^{18}O_c$ contrast evolution from 400 to 600 m decouples from the density contrast because of the deglacial change of AAIW, which distorts the relation between $\delta^{18}O_w$ and salinity. Therefore, water mass properties need to be better constrained before using the basin-wide $\delta^{18}O_c$ gradient to reconstruct density gradient, especially in the South Atlantic.

There are two cautionary notes on the North Atlantic cross-basin contrast here. First, previous studies suggest that the temperature, salinity, and $\delta^{18}O_w$ are quite different at 40°N due to the influence of the Mediterranean Outflow Water (MOW), complicating using the basin-wide $\delta^{18}O_c$ contrast to reconstruct the density contrast in the North Atlantic (Lynch-Stieglitz et al., 2008). Unfortunately, there is no MOW in C-iTRACE because of the closed Gibraltar Strait in the coarse resolution iPOP2 here. Therefore, the influence of the MOW cannot be quantified in our model, and we cannot comment on the use of $\delta^{18}Oc$ to reconstruct the density in regions influenced by MOW. Second, our model resolution is very coarse, 3° in the longitudinal direction. This coarse resolution produces a more diffusive WBC than in the real world. Therefore, further studies with higher resolution and with the inclusion of active MOW should be carried out to better assess the $\delta^{18}O$ contrast hypothesis.

In spite of these potential deficiencies, the C-iTRACE simulation provides the first systematic assessment of the $\delta^{18}O$ contrast hypothesis. Our study suggests that the density contrast across both the WBC region and the Atlantic basin can serve as a robust proxy for reconstructing the evolution of the past AMOC transport. Therefore, the development of accurate and independent temperature and salinity reconstructions has great potential to improve the AMOC reconstruction in the future. Furthermore, the reconstruction of cross-basin $\delta^{18}O_c$ contrasts over a large range of upper ocean depths in the Atlantic can also serve as a good proxy for AMOC evolution.

References

Boyle, E. A., & Keigwin, L. (1987). North Atlantic thermohaline circulation during the past 20,000 years linked to high-latitude surface temperature. *Nature*. https://doi.org/10.1038/330035a0

Bradtmiller, L. I., McManus, J. F., & Robinson, L. F. (2014). 231Pa/230Th evidence for a weakened but persistent Atlantic meridional overturning circulation during Heinrich Stadial 1. *Nature Communications*, *5*(5817). https://doi.org/10.1038/ncomms6817

Chase, Z., Anderson, R. F., Fleisher, M. Q., & Kubik, P. W. (2002). The influence of particle composition and particle flux on scavenging of Th, Pa and Be in the ocean. *Earth and Planetary Science Letters*, *204*(1–2), 215–229. https://doi.org/10.1016/S0012-821X(02)00984-6

Clark, P. U., Pisias, N. G., Stocker, T. F., & Weaver, A. J. (2002). The role of the thermohaline circulation in abrupt climate change. *Nature*, *415*(6874), 863–869. https://doi.org/10.1126/science.1081056

Clark, P. U., Shakun, J. D., Baker, P. A., Bartlein, P. J., Brewer, S., Brook, E. J., et al. (2012). Global climate evolution during the last deglaciation. *Proceedings of the National Academy of Sciences of the United States of America*, *109*(19), 1134–1142. https://doi.org/10.1073/pnas.1116619109/-/DCSupplemental.www.pnas.org/cgi/doi/10.1073/pnas.1116619109

Cunningham, S. a., Kanzow, T., Rayner, D., Baringer, M. O., Johns, W. E., Marotzke, J., et al. (2007). Temporal variability of the Atlantic Meridional Overturning Circulation at 26.5N. *Science*, *317*(5840), 935–938. https://doi.org/10.1126/science.1141304

Curry, W. B., & Oppo, D. W. (2005). Glacial water mass geometry and the distribution of δ 13 C of ΣCO 2 in the western Atlantic Ocean. *Paleoceanography*, *20*, PA1017. https://doi.org/10.1029/2004PA001021

Danabasoglu, G., Bates, S. C., Briegleb, B. P., Jayne, S. R., Jochum, M., Large, W. G., et al. (2012). The CCSM4 ocean component. *Journal of Climate*, *25*(5), 1361–1389. https://doi.org/10.1175/JCLI-D-11-00091.1

Evans, H. K., & Hall, I. R. (2008). Deepwater circulation on Blake Outer Ridge (western North Atlantic) during the Holocene, Younger Dryas, and Last Glacial Maximum. *Geochemistry, Geophysics, Geosystems*, *9*, Q03023. https://doi.org/10.1029/2007GC001771

Gebbie, G., & Huybers, P. (2006). Meridional circulation during the Last Glacial Maximum explored through a combination of South Atlantic δ18O observations and a geostrophic inverse model. *Geochemistry, Geophysics, Geosystems*, *7*, Q11N07. https://doi.org/10.1029/2006GC001383

Gherardi, J.-M., Labeyrie, L., Nave, S., Francois, R., McManus, J. F., & Cortijo, E. (2009). Glacial-interglacial circulation changes inferred from 231 Pa/230 Th sedimentary record in the North Atlantic region. *Paleoceanography*, *24*, PA2204. https://doi.org/10.1029/2008PA001696

Gu, S., & Liu, Z. (2017). 231Pa and 230Th in the ocean model of the Community Earth System Model (CESM1. 3). *Geoscientific Model Development*, *10*, 4723–4742. Retrieved from. http://doi.wiley.com/10.5194/gmd-10-4723-2017

Gu, S., Liu, Z., Zhang, J., Rempfer, J., Joos, F., & Oppo, D. W. (2017). Coherent response of Antarctic Intermediate Water and Atlantic Meridional Overturning Circulation during the last deglaciation: reconciling contrasting neodymium isotope reconstructions from the tropical Atlantic. *Paleoceanography*, *32*, 1036–1053. https://doi.org/10.1002/2017PA003092

Hirschi, J. J.-M., & Lynch-Stieglitz, J. (2006). Ocean margin densities and paleoestimates of the Atlantic meridional overturning circulation: A model study. *Geochemistry, Geophysics, Geosystems*, *7*, Q10N04. https://doi.org/10.1029/2006GC001301

Hirschi, J., & Marotzke, J. (2007). Reconstructing the meridional overturning circulation from boundary densities and the zonal wind stress. *Journal of Physical Oceanography*, *37*(3), 743–763. https://doi.org/10.1175/JPO3019.1

Jahn, A., Lindsay, K., Giraud, X., Gruber, N., Otto-Bliesner, B. L., Liu, Z., & Brady, E. C. (2015). Carbon isotopes in the ocean model of the Community Earth System Model (CESM1). *Geoscientific Model Development*, *8*(8), 2419–2434. https://doi.org/10.5194/gmd-8-2419-2015

Keigwin, L. D., & Lehman, S. J. (1994). Deep circulation change linked to HEINRICH Event 1 and Younger Dryas in a middepth North Atlantic Core. *Paleoceanography*, *9*(2), 185–194. https://doi.org/10.1029/94PA00032

Lea, D. W., & Boyle, E. A. (1990). Foraminiferal reconstruction of barium distributions in water masses of the glacial oceans. *Paleoceanography*, *5*(5), 719–742. https://doi.org/10.1029/PA005i005p00719

LeGrand, P., & Wunsch, C. (1995). Constraints from palaeo-tracer data on the North Atlantic circulation during the last glacial maximum. *Paleoceanography*, *10*(6), 1011–1045.

Lippold, J., Luo, Y., Francois, R., Allen, S. E., Gherardi, J., Pichat, S., et al. (2012). Strength and geometry of the glacial Atlantic Meridional Overturning Circulation. *Nature Geoscience*, *5*(11), 813–816. https://doi.org/10.1038/ngeo1608

Liu, Z., Lu, Z., Wen, X., Otto-Bliesner, B. L., Timmermann, A., & Cobb, K. M. (2014). Evolution and forcing mechanisms of El Niño over the past 21,000 years. *Nature*, *515*(7528), 550–553. https://doi.org/10.1038/nature13963

Liu, Z., Otto-Bliesner, B. L., He, F., Brady, E. C., Tomas, R., Clark, P. U., et al. (2009). Transient simulation of last deglaciation with a new mechanism for Bolling-Alllerod warming. *Science (New York, N.Y.)*, *325*(5938), 310–314. https://doi.org/10.1126/science.1171041

Liu, Z., Wen, X., Brady, E. C., Otto-Bliesner, B., Yu, G., Lu, H., et al. (2014). Chinese cave records and the East Asia Summer Monsoon. *Quaternary Science Reviews*, *83*, 115–128. https://doi.org/10.1016/j.quascirev.2013.10.021

Lynch-Stieglitz, J., Adkins, J. F., Curry, W. B., Dokken, T., Hall, I. R., Herguera, J. C., et al. (2007). Atlantic meridional overturning circulation during the Last Glacial Maximum. *Science (New York, N.Y.)*, *316*(5821), 66–69. https://doi.org/10.1126/science.1137127

Lynch-Stieglitz, J., Curry, W. B., Oppo, D. W., Ninneman, U. S., Charles, C. D., & Munson, J. (2006). Meridional overturning circulation in the South Atlantic at the last glacial maximum. *Geochemistry, Geophysics, Geosystems*, *7*, Q10N03. https://doi.org/10.1029/2005GC001226

Lynch-Stieglitz, J., Curry, W. B., & Slowey, N. (1999a). A geostrophic transport estimate for the Florida Current from the oxygen isotope composition of benthic foraminifera. *Paleoceanography*, *14*(3), 360–373. https://doi.org/10.1029/1999PA900001

Lynch-Stieglitz, J., Curry, W. B., & Slowey, N. (1999b). Weaker Gulf Stream in the Florida straits during the Last Glacial Maximum. *Nature*, *402*(6762), 644–648. https://doi.org/10.1038/45204

Lynch-Stieglitz, J., Hirschi, J. J.-M., Marchal, O., & Ninnemann, U. (2008). Prospects for reconstructing the Atlantic meridional overturning from cross-basin density estimates. *PAGES News*, *16*(1), 28–29. https://doi.org/10.1029/2006GC001383

Lynch-Stieglitz, J., Schmidt, M. W., & Curry, W. B. (2011). Evidence from the Florida Straits for Younger Dryas ocean circulation changes. *Paleoceanography*, *26*, PA1205. https://doi.org/10.1029/2010PA002032

Lynch-Stieglitz, J., Schmidt, M. W., Henry, G. L., Curry, W. B., Skinner, L. C., Mulitza, S., et al. (2014). Muted change in Atlantic overturning circulation over some glacial-aged Heinrich events. *Nature Geoscience*, *7*(2), 144–150. https://doi.org/10.1038/ngeo2045

Marchal, O., François, R., Stocker, T. F., & Joos, F. (2000). Ocean thermohaline circulation and sedimentary 231Pa/230Th ratio. *Paleoceanography*, *15*(6), 625–641. https://doi.org/10.1029/2000PA000496

Marchitto, T., Oppo, D. W., & Curry, W. B. (2002). Paired benthic foraminiferal Cd/Ca and Zn/Ca evidence for a greatly increased presence of Southern Ocean Water in the glacial North Atlantic. *Paleoceanography*, *17*(3), 1038. https://doi.org/10.1029/2000PA000598

Marchitto, T. M., & Broecker, W. S. (2006). Deep water mass geometry in the glacial Atlantic Ocean: A review of constraints from the paleonutrient proxy Cd/Ca. *Geochemistry, Geophysics, Geosystems*, *7*, Q12003. https://doi.org/10.1029/2006GC001323

Marchitto, T. M., Curry, W. B., Lynch-Stieglitz, J., Bryan, S. P., Cobb, K. M., & Lund, D. C. (2014). Improved oxygen isotope temperature calibrations for cosmopolitan benthic foraminifera. *Geochimica et Cosmochimica Acta*, *130*, 1–11. https://doi.org/10.1016/j. gca.2013.12.034

Marcott, S. A., Clark, P. U., Padman, L., Klinkhammer, G. P., Springer, S. R., Liu, Z., et al. (2011). Ice-shelf collapse from subsurface warming as a trigger for Heinrich events. *Proceedings of the National Academy of Sciences*, *108*(33), 13,415–13,419. https://doi.org/ 10.1073/pnas.1104772108

McManus, J., Francois, R., & Gherardi, J. (2004). Collapse and rapid resumption of Atlantic meridional circulation linked to deglacial climate changes. *Nature*, *428*(6985), 834–837.

Moreno-Chamarro, E., Ortega, P., González-Rouco, F., & Montoya, M. (2017). Assessing reconstruction techniques of the Atlantic Ocean circulation variability during the last millennium. *Climate Dynamics*, *48*(3–4), 799–819. https://doi.org/10.1007/s00382-016-3111-x

Olbers, D., Gouretski, V., Seib, G., & Schroter, J. (1992). Hydrographic Atlas of the Southern Ocean. *Alfred Wegener Institute., Bremerhaven, Germany*, *17 pp and*.

Otto-Bliesner, B. L., Russell, J. M., Clark, P. U., Liu, Z., Overpeck, J. T., Konecky, B., et al. (2014). Coherent changes of southeastern equatorial and northern African rainfall during the last deglaciation. *Science*, *346*(6214), 1223–1227. https://doi.org/10.1126/ science.1259531

Sarkisyan, A. S., & Ivanov, V. F. (1971). Joint effect of baroclinicity and bottom relief as an important factor in the dynamics of the sea current. *Investiya Academy of Sciences, USSR, Atmospheric and Ocean Sciences (English Trans)*, *1*, 173–188.

Schmitz William, J. J., & McCartney, M. S. (1993). On the North Atlantic circulation. *Reviews of Geophysics*, *31*(1), 29–49.

Sverdrup, H. U. (1947). Wind-driven currents in a baroclinic ocean; with application to the equatorial currents of the eastern Pacific. *Proceedings of the National Academy of Sciences*, *33*, 318–326.

Yu, E.-F., Francois, R., & Bacon, M. P. (1996). Similar rates of modern and last-glacial ocean thermohaline circulation inferred from radiochemical data. *Nature*. https://doi.org/10.1038/379689a0

Zhang, J., Liu, Z., Brady, E. C., Jahn, A., Oppo, D. W., Clark, P. U., et al. (2017). Asynchronous warming and oxygen isotope evolution of deep Atlantic water masses during the last deglaication. *Proceedings of the National Academy of Sciences*, *114*(42), 11075–11080. https:// doi.org/10.1073/pnas.1704512114